Available online at www.sciencedirect.com
ScienceDirect
Acta Materialia 57 (2009) 4133–4139
Acta MATERIALIA
www.elsevier.com/locate/actamat

Structural evolution of Cu–Zr metallic glasses under tension

N. Mattern [a,*], J. Bednarčik [b], S. Pauly [a], G. Wang [a], J. Das [c], J. Eckert [a,d]

[a] IFW Dresden, Institute for Complex Materials, P.O. Box 270116, D-01071 Dresden, Germany
[b] HASYLAB at DESY, Notkestr. 85, D-22603 Hamburg, Germany
[c] IIT Kharagpur, Department of Metallurgical and Materials Engineering, Kharagpur 721302, West Bengal, India
[d] TU Dresden, Institute of Materials Science, D-01062 Dresden, Germany

Received 15 April 2009; received in revised form 7 May 2009; accepted 8 May 2009
Available online 10 June 2009

Abstract

The structural behaviour of $Cu_{50}Zr_{50}$ and $Cu_{65}Zr_{35}$ metallic glasses under uniaxial tensile stress was investigated in situ by high-energy X-ray synchrotron diffraction. The components of the elastic strain tensor were determined from both the change of positions of first maximum of the structure factor in reciprocal space as well as from the maxima of the atomic pair correlation function in real space. The atomic scale strain agrees with the macroscopic strain values. The topological and chemical short-range order of the Cu–Zr glasses changes upon loading. The number density of Cu–Zr and Zr–Zr nearest neighbour atomic pair becomes oriented along the loading direction whereas the partial nearest neighbour distances are only weakly influenced.
© 2009 Acta Materialia Inc. Published by Elsevier Ltd. All rights reserved.

Keywords: Metallic glasses; Short-range order; Cu–Zr; Mechanical properties

1. Introduction

Poulsen et al. have demonstrated that the strain tensor of bulk metallic glasses (BMGs) can be quantitatively estimated by using high-energy X-ray synchrotron diffraction [1]. Similar to the well-established method for strain analysis of crystalline materials, the direction-dependent relative shift of the diffraction peaks in reciprocal space can be used to determine the components of the strain tensor and elastic moduli, or analogously in real space the change of the maxima positions of the atomic pair distribution function (PDF), respectively. Hufnagel et al. reported that the strain values in a metallic glass measured by X-ray diffraction (XRD) is in good agreement with macroscopic observations of their elastic behaviours [2]. Deviations in the elastic moduli between different methods are about 5–10%. Furthermore, in situ diffraction measurements have been carried out for Cu–Zr–Al and Zr–Cu–Ni–Al–Ti BMGs in compression [3] or tension [4,5]. In all this work, the PDFs were calculated using the sine-Fourier transformation of the structure factor. Dmowski et al. [6] pointed out that in the presence of structural anisotropy, it is necessary to expand the PDF into spherical harmonics as introduced in Refs. [7,8], otherwise systematic errors may occur especially in the first neighbourhood.

In this work, we report on the structural evolution of $Cu_{50}Zr_{50}$ and $Cu_{65}Zr_{35}$ metallic glasses under tension. The experimental results will show changes in the short-range order under applied stress within the elastic regime well below the yield stress.

2. Experimental

$Cu_{50}Zr_{50}$ and $Cu_{65}Zr_{35}$ glassy ribbons of 7 mm in width were prepared by rapid quenching from the melt by planar casting on a rotating copper wheel. Dog-bone-shaped samples were prepared with to 4 mm in width. The areas of the cross-section of the ribbons ($A = 0.216\ mm^2$ for the $Cu_{50}Zr_{50}$ glass, and $A = 0.176\ mm^2$ for the $Cu_{65}Zr_{35}$ glass)

* Corresponding author. Tel.: +49 3514659367; fax: +49 3514659452.
E-mail address: n.mattern@ifw-dresden.de (N. Mattern).

1359-6454/$36.00 © 2009 Acta Materialia Inc. Published by Elsevier Ltd. All rights reserved.
doi:10.1016/j.actamat.2009.05.011

were determined by optical microscopy equipped with an image analyser QTM550. The specimens were loaded under tension by using a straining system with a maximum load of 5 kN (Kammrath and Weiss GmbH). High-energy X-ray diffraction at Hasylab BW5 beamline was applied to analyze the structural evolution under load. Additional, macroscopic elongation was measured by a laser extensometer attached to an Instron machine. The layout of the diffraction experiments is schematically shown in Fig. 1. The stressed samples were exposed for 10 s at a particular load to the well collimated incident beam having a spot size of $1 \times 1\ mm^2$. XRD patterns were collected in symmetric transmission geometry using a MAR 345 two-dimensional (2D) image plate detector (2300×2300 pixels, $150 \times 150\ \mu m^2$ pixel size), which was carefully mounted perpendicular to the incident X-ray beam. The wavelength $\lambda = 0.01265$ nm facilitates to acquire intensities up to large values ($\sim 160\ nm^{-1}$) of the scattering vector $q(q = 4\pi \sin\theta/\lambda)$. The load was increased in steps until the sample was fractured. In order to get better statistics of the results, each measurement was repeated several times. The highest load before fracture was measured to be $L = 160$ N for $Cu_{50}Zr_{50}$ glass which corresponds to an applied stress of $\sigma = 741$ MPa well below the yield strength of 1.6 GPa reported for Cu–Zr BMGs [9] ($L = 140$ N was the highest load for the $Cu_{65}Zr_{35}$ glass). The two-dimensional diffraction patterns were recorded at three different positions along the length of the ribbon. No differences were found between the 2D diffraction patterns captured at different positions of the samples. The circular–elliptical diffraction patterns were characterized with respect to the polar coordinates $I(q, \chi)$. From the 2D intensity distribution, 36 sections $I(q, \chi)$ were extracted with an integration $\pm 5°$ in χ by Fit2D program [10]. The intensity curves $I(q, \chi)$ were corrected by considering background, polarization, inelastic

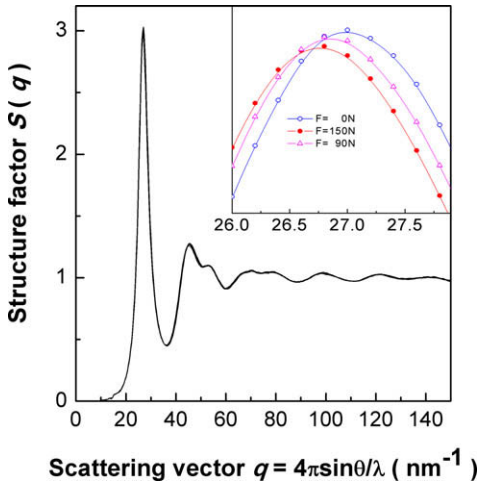

Fig. 2. Structure factor $S(q, \chi = 0°)$ of $Cu_{50}Zr_{50}$ metallic glass as a function of load.

Compton scattering and then transformed into the structure factor $S(q, \chi)$ by normalizing in absolute electron units [11].

3. Results

3.1. Reciprocal space data

Fig. 2 shows the structure factor $S(q, \chi = 0°)$ of $Cu_{50}Zr_{50}$ glass measured along the loading direction. Small changes occur in the positions of the maxima upon loading. The position of the first maximum q_1 at about $27\ nm^{-1}$ is shifted to lower q-values whereas, along the perpendicular direction ($\chi = 90°$), q_1 moves to higher q-values as expected. It has already been reported [1,2] that the relative change of the position of the first maximum can be used to determine the atomic scale strain. However, no relationship

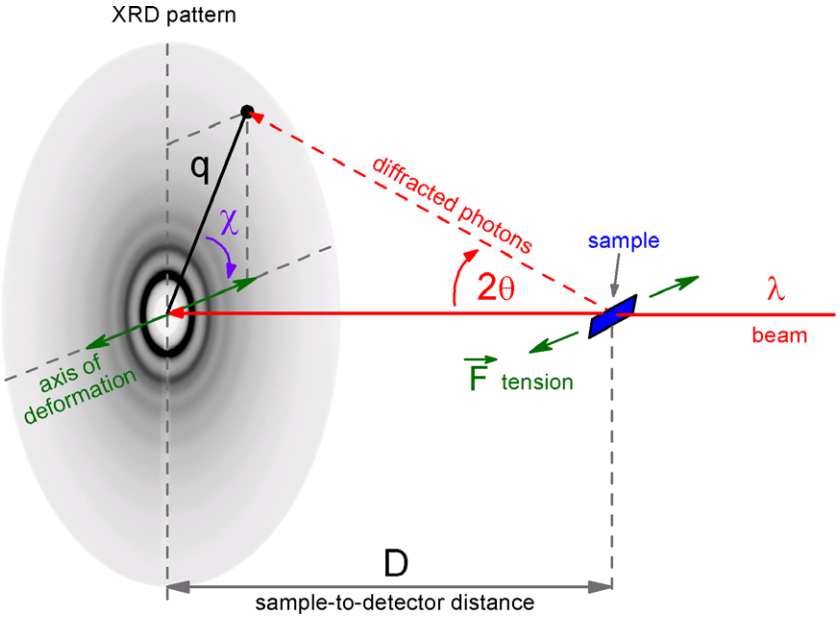

Fig. 1. Experimental setup for in situ X-ray diffraction under applied load.

exists between the maxima in reciprocal and in real space for amorphous materials due to the absence of translation symmetry. This method assumes that all inter-atomic distances of a direction are altered by the same factor upon stress, and no other structural changes occur. The angular dependent strain is then given by:

$$\varepsilon(\sigma,\chi) = \frac{q_1(0,\chi) - q_1(\sigma,\chi)}{q_1(\sigma,\chi)} \quad (1)$$

Fig. 3 shows the calculated strain values of the $Cu_{50}Zr_{50}$ glass as a function of direction χ at different loads. The angle dependence of $\varepsilon(\sigma, \chi)$ reflects the symmetry of the uniaxial stress state. The values vary from tensile strain for $\chi = 0°$ to compressive strain for $\chi = 90°$. The strain curves for the different loads intersect at $\chi = 54.7°$ in accordance with the strain-free direction ($\varepsilon(\sigma, \chi = 54.7°) = 0$). From the measured angular variation of the strain the component of the strain tensor ε_{ij} were calculated by a least square fit of:

$$\varepsilon(\sigma,\chi) = \varepsilon_{11}\cos^2\chi + \varepsilon_{12}\sin\chi\cos\chi + \varepsilon_{22}\sin^2\chi \quad (2)$$

The corresponding fit curves are given in Fig. 3 as marked by dashed lines. Fig. 4 shows the variation of axial (ε_{11}), tangential (ε_{22}) and in-plane shear component (ε_{12}) with stress. A linear behaviour of the strain with applied stress is observed up to the highest value before fracture. The Young's modulus $E = 63$ GPa and the Poisson' ratio $v = 0.31$ can be directly obtained from the slopes of the axial and tangential components ε_{11} and ε_{22} vs. stress. The shear modulus $G = 24$ GPa follows from $G = E/2(1+v) = 0.382E$. The XRD values agree well with the macroscopic tensile measurement as shown in Fig. 4. In the case of the $Cu_{65}Zr_{35}$ glass similar linear dependence of strain with stress were obtained. The calculated values of the elastic moduli are summarized in Table 1. The relative error is estimated to be about 10% mainly due to the uncertainty of cross-section determination. Considering that, the data are in good agreement with data reported for Cu–Zr BMGs in the literature [12–14].

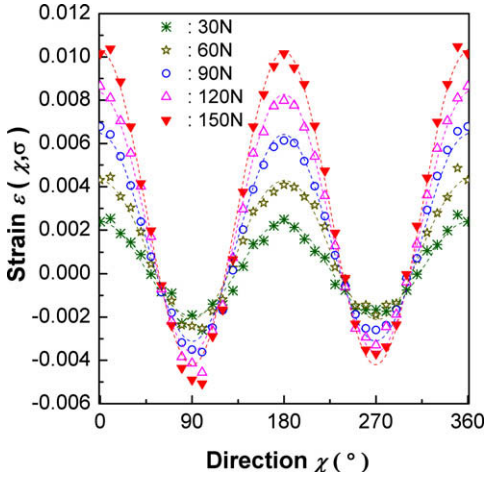

Fig. 3. Direction dependence of the strain $\varepsilon(\sigma, \chi)$ of $Cu_{50}Zr_{50}$ metallic glass (dashed lines represent fit of Eq. (2)).

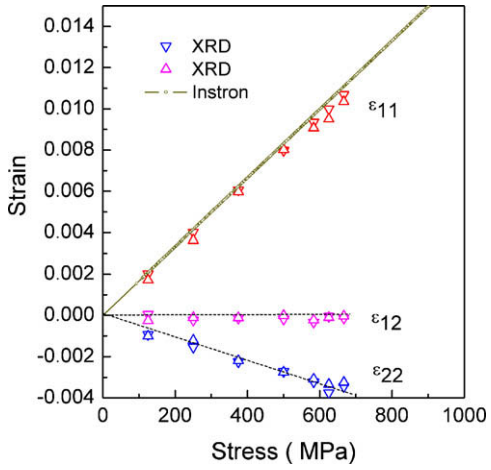

Fig. 4. Strain vs. applied stress of $Cu_{50}Zr_{50}$ glass measured by XRD and mechanical testing.

Usually the atomic structure of amorphous materials is isotropic. However in the presence of stress the structure factor becomes anisotropic. In such a situation, the direction dependence of the structure factor $S(\vec{q})$ can be described by the expansion into spherical harmonics as reported in the literature [6–8]:

$$S(\vec{q}) = \sum_{l,m} S_l(q) Y_l(\vec{q}/q) \quad (3)$$

For the uniaxial cylinder symmetry the spherical harmonics Y are reduced to the Legendre polynomials:

$$Y_l(\chi) = \sqrt{\frac{2l+1}{4\pi}} P_l(\cos\chi) \quad (4)$$

Neglecting higher-order terms $l > 2$ (their contributions were estimated to be one order of magnitude lower than those of $l = 2$), the structure factor of any direction χ is given by:

Table 1
Young's modulus E, Poisson ratio v, and shear modulus G of Cu–Zr glasses.

	Young's modulus E (GPa)	Poisson ratio (v)	Shear modulus G (GPa)	
$Cu_{50}Zr_{50}$	63	0.31	24	This work[a]
	59			This work[b]
	83	0.38	30	[9]
	82 (78)			[13]
$Cu_{65}Zr_{35}$	97			This work[a]
	86	0.33	36	This work[b]
	92			[9]
	92	0.35	34	[12]
	115 (98)			[13]

[a] XRD.
[b] Electromechanical device.

$$S(q,\chi) = S_0(q)\sqrt{\frac{1}{4\pi}} + S_2(q)\cdot\sqrt{\frac{5}{16\pi}}\left(3\cos^2\chi - 1\right) \quad (5)$$

The components of the structure factor $S_0(q)$ and $S_2(q)$ can be calculated from the two measurements parallel ($\chi = 0°$) and perpendicular ($\chi = 90°$) to the tensile directions:

$$S_0(q) = \frac{\sqrt{4\pi}}{3}\left(S(q,\chi = 0°) + 2S(q,\chi = 90°)\right) \quad (6)$$

$$S_2(q) = \sqrt{\frac{16\pi}{45}}\cdot\left(S(q,\chi = 0°) - S(q,\chi = 90°)\right) \quad (7)$$

For $\chi = 54.7°$ the contribution of the anisotropic part demises and the isotropic structure factor can also be obtained by $S_0(q) = \sqrt{4\pi}S(q,\ \chi = 54.7°)$.

Fig. 5 compares the calculated isotropic structure factors $S_0(q)$ of $Cu_{50}Zr_{50}$ for the highest load (150 N) with that of without load (0 N). The difference curve S_0(150 N)–S_0(0 N) exhibits small changes of about 1% of the isotropic structure factor $S_0(q)$ occurring at the first maximum. The change of the isotropic part of the structure factor may originate from atomic rearrangements under stress as discussed later. The anisotropic part of the structure factor $S_2(q)$ is also given in Fig. 5. The amplitude of $S_2(q)$ increases gradually as function of the applied stress and reaches values up to 10% at the first maximum.

3.2. Real space data

For isotropic amorphous materials the atomic density functions $\rho(r)$ can be calculated by the sine-Fourier transform of the structure factor:

$$\rho(r) = \rho_{mean} + \frac{1}{2r\pi^2}\cdot\int (S(q) - 1)\cdot q\cdot\sin(q\cdot r)\cdot dq \quad (8)$$

where ρ_{mean} is the mean atomic density. For the uniaxial cylinder symmetry the direction dependent atomic density function $\rho(\vec{r})$ can be expressed by the expansion into spherical harmonics analogously to the structure factor [6–8]:

$$\rho(\vec{r}) = \sum_l \rho_l(r)Y_l(\vec{r}/r) \quad (9)$$

The components of the anisotropic PDF and the corresponding components of anisotropic structure factor are related by a transformation:

$$\rho_l(r) = \frac{i^l}{2\pi^2}\cdot\int S_l(q)\cdot J_l(qr)\cdot q^2 dq \quad (10)$$

where $J_l(x)$ is the lth order of the spherical Bessel function ($x = qr$).

For $l = 0$ the isotropic part of the atomic pair correlations ρ_0 (r) corresponds to Eq. (8) since $J_0(qr) = \frac{\sin(qr)}{qr}$. The anisotropic part of the atomic pair correlations $\rho_2(r)$ is obtained from the anisotropic part of the structure factor $S_2(q)$ by:

$$\rho_2(r) = -\frac{1}{2\pi^2}\cdot\sqrt{\frac{45}{16\pi}}\int S_2(q)\cdot J_2(qr)\cdot q^2 dq \quad (11)$$

$$\text{with } J_2(qr) = \left(\tfrac{2}{(qr)^3} - \tfrac{1}{qr}\right)\sin(qr) - \tfrac{2}{(qr)^2}\cos(qr)$$

The atomic density of any direction χ is then given by:

$$\rho(r,\chi) = \rho_0(r)\sqrt{\frac{1}{4\pi}} + \rho_2(r)\cdot\sqrt{\frac{5}{16\pi}}(3\cos\chi^2 - 1) \quad (12)$$

Fig. 6 compares the calculated atomic density functions $\rho(r,\ \chi)$ of the $Cu_{50}Zr_{50}$ glass in tensile direction ($\chi = 0°$) with and without stress. The maxima of the pair correlation function shift to larger inter-atomic distances due to the applied load of $F = 150$ N. Besides the shift of the maxima positions, the shape of the first maximum corresponding to the nearest neighbourhood is changed. The positions of the maxima of $\rho(r,\ \chi)$ were determined by a fit to the Gaussian function. The relative shift of the different maxima r_i of the PDFs is shown in Fig. 7.

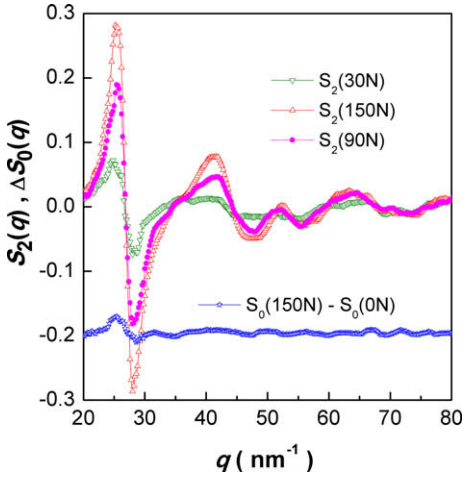

Fig. 5. Change of isotropic structure factor S_0 vs. load and anisotropic structure factor S_2 of $Cu_{50}Zr_{50}$ glass.

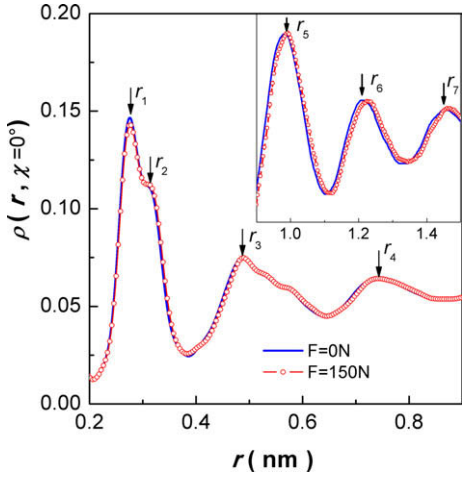

Fig. 6. Atomic density $\rho(r,\ \chi = 0)$ of $Cu_{50}Zr_{50}$ glass in the tensile direction vs. load.

The values

$$\varepsilon(\sigma,\chi) = \frac{r_i(\sigma,\chi) - r_i(0,\chi)}{r_i(\sigma,\chi)}$$

define the direction-dependent strain in the atomic scale. The calculated strain values behave quite similar for the maxima at $r > 0.4$ nm. The accuracy of position determination in real space is reduced due to the broad maxima of the PDFs which is probably the reason for the enhanced scatter. The slopes are in reasonable agreement with those of the in reciprocal space (Fig. 4).

The anisotropic part of the PDF is shown in Fig. 8 for two different values of the applied load. The amplitude of $\rho_2(r)$ increases gradually with stress, which is similar to the anisotropic structure factor $S_2(q)$ (Fig. 5). It should be noted that in the case of pure elastic deformation the anisotropic PDF part should be proportional to the first deviate of the isotropic PDF as discussed by Suzuki et al. [7]:

$$\rho_2^*(r) = -\sqrt{\frac{16\pi}{45}} \cdot r \cdot \frac{d\rho_0}{dr}\varepsilon \tag{13}$$

The corresponding curve of $\rho_2^*(r)$ at a strain of $\varepsilon = 0.01$ is given in Fig. 8. The differences between $\rho_2^*(r)$ and $\rho_2(r)$ can be identified for the first neighbourhood. However, at $r > 0.4$ nm the contributions of the anisotropic atomic density are rather negligible. The deviation of the experimentally determined $\rho_2(r)$ indicates the structural change in the short-range order due to the application of load. Fig. 9a–d compares the direction dependences of first maximum of the PDF of the Cu–Zr glasses for $\chi = 0°$ and $\chi = 90°$ as a function of the load. For the Cu–Zr metallic glasses the $\rho(r)$ curves represent the weighted sum the three partial atomic pair correlation functions ρ_{CuCu}, ρ_{CuZr}, ρ_{ZrZr}. The visible two components of the PDF can be attributed to the partial zirconium–copper ($r^1_{ZrCu} = 0.27$ nm) and zirconium–zirconium ($r^1_{ZrZr} = 0.32$ nm) pair correlations. The different heights of the contributions of $Cu_{50}Zr_{50}$ and $Cu_{65}Zr_{35}$ glasses (Fig. 9a and c) are due to the composition dependence of the weighting factors partial functions. Fig. 9a and c compare the first maximum of the PDFs of the unloaded Cu–Zr glasses for the two directions $\chi = 0°$ and $\chi = 90°$, respectively. For an isotropic structure the curves should be identical. The agreement is a measure for the relative errors in the determination of inter-atomic distances and coordination numbers given in Table 2. Fig. 9b shows the nearest neighbourhood of the $Cu_{50}Zr_{50}$ glass under applied stress ($L = 150$ N) in tensile ($\chi = 0°$) and perpendicular direction ($\chi = 90°$). Differences in position and height of the two components are visible. The values of the positions r_i and the area N_i of the two components were determined by a fit of two Gaussian functions. The results are summarized in Table 2. The positions of the two maxima corresponding to the nearest neighbour distances Cu–Zr and Zr–Zr increase along the tensile direction and decrease in the perpendicular direction. The relative shift for both cases is given in Table 2, which is much lower than that of the maxima at larger inter-atomic distances resulting in a much lower value if a strain ε^* is calculated. These experimentally observed deviations between nearest neighbours and correlations maxima at larger distances was also reported in the literature for other metallic glasses [1,2,4,5]. Such a change confirms the anelastic atomic rearrangements in topologically unstable regions, as proposed for creep-deformed metallic glasses [7,8]. Beside the change of the nearest neighbour distances, the intensities of the components are found to be different for the two directions which reflect the anisotropic part of the PDF (Fig. 8). From the analysis of the first maximum it follows that the number of Zr–Zr neighbours increases in tensile direction, and the number of Cu–Zr pairs decreases, respectively. The opposite behaviour is found for the perpendicular direction. The total number $N^1_{ZrCu} + N^1_{ZrZr}$ remains constant. The same tendency is observed for the $Cu_{65}Zr_{35}$ glass under tension as shown in Fig. 9d (Table 2).

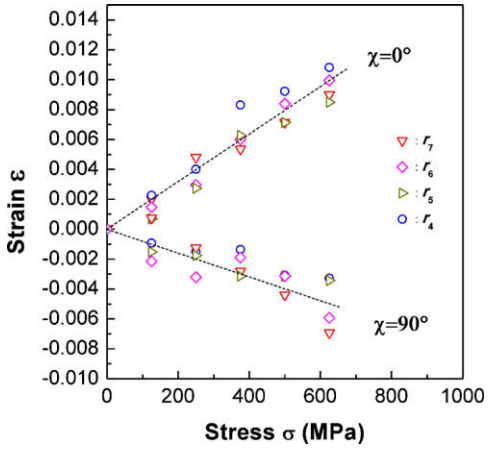

Fig. 7. Strain vs. applied load of $Cu_{50}Zr_{50}$ glass determined from the shift of maxima positions r_i of $\rho(r, \chi)$.

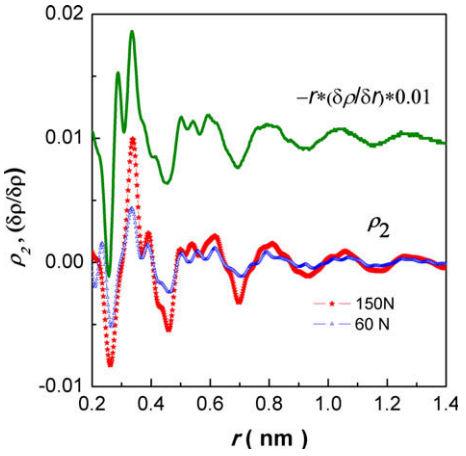

Fig. 8. Anisotropic PDFs $\rho_2(r)$ and first derivative of $\rho_0(r)$ of $Cu_{50}Zr_{50}$ glass.

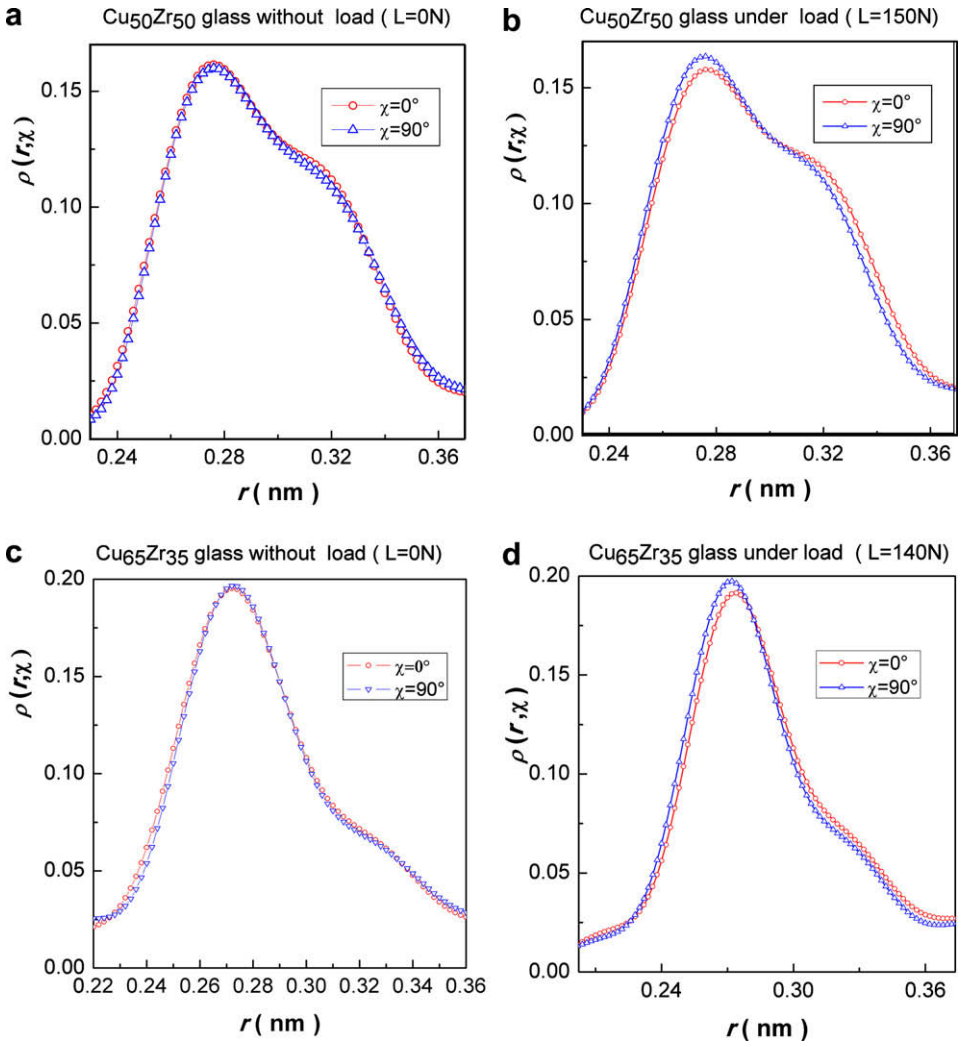

Fig. 9. Direction dependence of nearest neighbourhood of Cu–Zr glasses: (a) $Cu_{50}Zr_{50}$ glass without stress, (b) $Cu_{50}Zr_{50}$ glass under tensile stress, (c) $Cu_{65}Zr_{35}$ glass without stress and (d) $Cu_{65}Zr_{35}$ glass under tensile stress.

Table 2
Direction-dependent distances r_i, strain ε^* and coordination numbers N_i of nearest neighbourhood in Cu–Zr glasses under tensile stress.

	$Cu_{50}Zr_{50}$			$Cu_{65}Zr_{35}$		
	$L = 0$ N $\rho_0(r)$	$L = 150$ N $\rho(r, \chi = 0°)$	$L = 150$ N $\rho(r, \chi = 90°)$	$L = 0$ N $\rho_0(r)$	$L = 140$ N $\rho(r, \chi = 0°)$	$L = 140$ N $\rho(r, \chi = 90°)$
r_1 (nm)	0.2734 ± 0.0003	0.2745	0.2733	0.2711	0.2726	0.2705
ε^*	–	0.004	−0.0004	–	0.006	−0.002
r_2(nm)	0.3189 ± 0.0003	0.3209	0.3183	0.3220	0.3248	0.3215
ε^*	–	0.006	−0.002	–	0.009	−0.002
N_1	6.1 ± 0.2	5.9	6.2	9.6	9.5	9.6
N_2	8.0 ± 0.2	8.4	7.8	4.2	4.4	4.1
$N_1 + N_2$	14.1 ± 02	14.3	14.0	13.8	13.9	13.7

4. Discussion

In a glassy material a range of local atomic environments of the atoms exists. As a consequence of the disorder, fluctuation of inter-atomic distances, occur which leads to variations of the atomic-level stress [14]. Molecular dynamic simulations (MD) under stress showed that atomic rearrangements take place during loading in a few topologically unstable regions [15]. Suzuki et al. [7] explained for creep experiments the induced structural anisotropy by a bond reorientation model. Argon [16] proposed a flow model for plastic deformation of metallic glasses by local shear transformation of atomic clusters of so-called shear transformation zones (STZ). Recent MD calculations for $Cu_{54}Zr_{46}$ glass report on the movement and rearrangement of atomic polyhedra under tensile

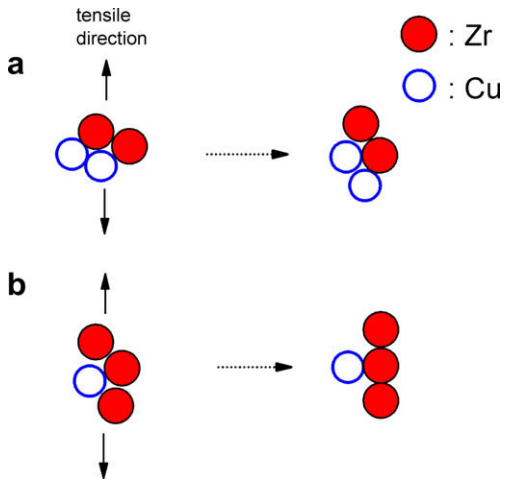

Fig. 10. Schematic representation of local atomic rearrangements under applied load.

strain [17] in the structure model in the elastic as well as in the plastic regime. Our analysis of the first neighbourhood confirms the anelastic changes of the short-range order under tensile stress well below the yield strength. The response of the nearest neighbourhood upon loading points to directional changes in the chemical short-range order. It is reported [13,17,18] that Cu–Zr glasses consist of densely packed atomic polyhedra arrangements. In the metastable equilibrium the spatial orientations of the polyhedra averages out. Under external stress certain atoms rearrange in order to accommodate the elastic strain along the loading axis. One possible mechanism for such transformation could be local diffuse movement or reshuffling of atoms and bond reorientations [7]. Fig. 10a and b shows schematically such atomic rearrangements resulting in a directional altered short-range order. Upon loading the number Zr–Zr atoms may locally increase in the tensile direction (Fig. 10b) while the number of Cu–Zr neighbours increases perpendicular to the tensile direction (Fig. 10a and b). Another possible explanation of the observed changes in the short-range order could be local shear events which can take place even below the yield strength [19]. The transformations may occur only in certain clusters with corresponding local structure, stress state, and orientation to the stress direction. So locally bond reorientations happen in a limited number of clusters and such events spread to the overall structure with increasing stress.

5. Conclusions

In situ X-ray synchrotron diffraction enables the atomic level elastic strain of metallic glasses under uniaxial tensile stress to be characterized. The elastic moduli can be estimated not only considering the shift of the first maximum of the scattering curve in reciprocal space but also from the shift of the larger inter-atomic distances in the PDF in real space. The analysis of the short-range order of $Cu_{50}Zr_{50}$ and $Cu_{65}Zr_{35}$ glasses vs. stress confirms the structural changes in the elastic regime well below the yield strength. These anelastic deformations are accompanied by bond reorientation leading to direction dependent changes in chemical short-range order. The number of Zr–Zr pairs increases along the tensile direction whereas Cu–Zr pairs decreases with applied stress. To evaluate the proposed deformation mechanism further MD calculations of Cu–Zr under tensile and compressive stress are necessary with a combined direction dependent structure analysis of the model. Experimentally, the determination of partial PDFs under applied stress should give more insight into the structural response of metallic glasses during elastic deformation.

Acknowledgments

The authors are grateful for the financial support provided by the European Union within the framework of the Research Training Network on "ductile bulk metallic glass composites" (MRTN-CT-2003-504692). The Alexander von Humboldt Foundation is acknowledged for financial support of G. Wang.

References

[1] Poulsen HF, Wert JA, Neuefeind J, Honkimaki V, Daymond M. Nat Mater 2005;4:33.
[2] Hufnagel TC, Ott RT, Almer J. Phys Rev B 2006;73:064204.
[3] Das J, Bostrom M, Mattern N, Kvick A, Yavari AR, Greer AL, et al. Phys Rev B 2007;76:092203.
[4] Wang XD, Bednarcik J, Saksl K, Franz H, Cao QP, Jiang JZ. Appl Phys Lett 2007;91:081913.
[5] Stoica M, Das J, Bednarcik J, Franz H, Mattern N, Wang WH, et al. J Appl Phys 2008;104:013522.
[6] Dmowski W, Egami T. J Mater Res 2007;22:412.
[7] Suzuki Y, Haimovich J, Egami T. Phys Rev B 1987:35,2162.
[8] Egami T, Dmowski W, Kosmetatos P, Boord M, Tomida T, Oikawa E, et al. J Non-Cryst Solids 1995;193:591.
[9] Duan G, Blauwe K, Lind ML, Schramm JP, Johnson WL. Scripta Mater 2008;58:159.
[10] Hammersley AP, Svensson SO, Hanfland M, Fitch AN, Haeusermann D. High Press Res 1996;14:235. <http://www.esrf.eu/computing/scientific/FIT2D/>.
[11] Egami T, Billinge SJL. Underneath the Bragg peaks: structural analysis of complex materials. Oxford: Pergamon Press; 2003.
[12] Xu D, Lohwongwatana B, Duan G, Johnson WL, Garland C. Acta Mater 2004;52:2621.
[13] Park KW, Lee CM, Wakeda M, Shibutani J, Falk M, Lee JC. Acta Mater 2008;56:5440.
[14] Egami T, Maeda K, Vitek V. Philos Mag 1980;A41:883.
[15] Srolovitz D, Vitek V, Egami T. Acta Metall 1983;31:335.
[16] Argon AS, Kuo HY. J Non-Cryst Solid 1980;37:241.
[17] Lekka CE, Ibenskas A, Yavari AR, Evangelakis GA. Appl Phys Lett 2007;91:214103.
[18] Wang XD, Yin S, Cao QP, Jiang JZ, Franz H, Jin ZH. Appl Phys Lett 2008;92:011902.
[19] Lee SC, Lee CM, Lee JC, Kim HJ, Shibutani Y, Fleury E, et al. Appl Phys Lett 2008;92:151906.